MATERIALS SCIENCE

Long-term reliable physical health monitoring by sweat pore–inspired perforated electronic skins

Hanwool Yeon[1,2†], Haneol Lee[1,2,3†], Yeongin Kim[1,2†], Doyoon Lee[1,2], Youngjoo Lee[4], Jong-Sung Lee[5], Jiho Shin[1,2], Chanyeol Choi[2,6], Ji-Hoon Kang[1,2], Jun Min Suh[1,2,5], Hyunseok Kim[1,2], Hyun S. Kum[1,2], Jaeyong Lee[1,2], Daeyeon Kim[7], Kyul Ko[7], Boo Soo Ma[7], Peng Lin[1,2,8], Sangwook Han[1,2,5], Sungkyu Kim[1,2,9], Sang-Hoon Bae[1,2], Taek-Soo Kim[10], Min-Chul Park[7], Young-Chang Joo[5], Eunjoo Kim[11], Jiyeon Han[12,13]*, Jeehwan Kim[1,2,14]*

Electronic skins (e-skins)—electronic sensors mechanically compliant to human skin—have long been developed as an ideal electronic platform for noninvasive human health monitoring. For reliable physical health monitoring, the interface between the e-skin and human skin must be conformal and intact consistently. However, conventional e-skins cannot perfectly permeate sweat in normal day-to-day activities, resulting in degradation of the intimate interface over time and impeding stable physical sensing. Here, we present a sweat pore–inspired perforated e-skin that can effectively suppress sweat accumulation and allow inorganic sensors to obtain physical health information without malfunctioning. The auxetic dumbbell through-hole patterns in perforated e-skins lead to synergistic effects on physical properties including mechanical reliability, conformability, areal mass density, and adhesion to the skin. The perforated e-skin allows one to laminate onto the skin with consistent homeostasis, enabling multiple inorganic sensors on the skin to reliably monitor the wearer's health over a period of weeks.

INTRODUCTION

In the coming age of ubiquitous health monitoring, electronic skin (e-skin) represents one of the mainstream hardware innovations, enabling imperceptible and noninvasive health monitoring of human beings from the skin (*1*–*3*). Exciting progresses have been made in the field of e-skin–based health monitoring platforms including development of flexible/stretchable electronic circuits (*4*–*7*), skin-compatible adhesive patches (*8*–*10*), and their conformal lamination onto the skin. One of the crucial steps to advance this technology into the commercialization stage is to ensure long-term monitorability of physiological activities of our skins with high precision. Although improved flexibility/stretchability of the e-skin, by thinning down the thickness (*7*, *11*, *12*) and forming a mesh network (*1*, *6*), can enhance conformability on the skin, accumulation of skin by-products such as sweat at the skin/e-skin interface cannot be avoided in current state-of-the-art e-skins, thus hampering precise cutaneous sensing for an extended period of time. Although accumulated sweat at the e-skin/skin interface has been used as a biomarker of chemical sensors (*13*, *14*) and an energy source of fuel cells (*15*, *16*), long-term conformability is not secured because accumulated sweat could cause malfunction of the physical sensors (*11*) and eventually delaminate the e-skin from the human skin. This trapped skin by-product degrades homeostatic functions of the skin (e.g., skin barrier function), resulting in perturbation of skin health information that is critical for diagnosis of skin disorders (e.g., erythema) and internal diseases (e.g., allergies) (*17*). However, there is a lack of innovation on "sweat" permeable e-skins (see table S1). Allowing "vapor" permeation through e-skins by open-mesh electronic circuits with porous elastomeric adhesives (*8*, *10*, *18*) and nanofiber-based e-skins (*19*–*23*) can alleviate these problems, resulting in increasing monitorability of physiological activity (up to 7 days of skin compatibility and ≥10 hours of continuous monitorability at the best case). However, this gas-permeable path is not enough to prevent sweat trapping–induced monitoring failures. Furthermore, organic-based physical sensors are not desirable for long-term reliable monitoring because of their instability to environmental factors such as moisture (*24*). Therefore, to perform reliable cutaneous health monitoring for long-term period without limitation of human activities, it is ideal to obtain e-skins that contain sweat-permeable channels with stable inorganic sensors.

Here, we introduce a sweat pore–inspired fully perforated e-skin containing inorganic sensor arrays that unlocks the way to completely permeate profuse sweat through e-skins. This allows unprecedentedly long and reliable health monitoring for over a week while maintaining healthy state of the human skin. We found that under profuse sweat condition, a conventional e-skin not only delaminates from the skin but also does not accurately sense due to sensor malfunction. We successfully avoid these by forming engineered hole patterns through inorganic thin-film sensor modules as well as elastomer adhesives, where the patterns are precisely designed to avoid fully blocking the sweat pores on human skins. Simultaneously, perforation has been engineered to enhance physical

[1]Department of Mechanical Engineering, Massachusetts Institute of Technology, Cambridge, MA 02139, USA. [2]Research Laboratory of Electronics, Massachusetts Institute of Technology, Cambridge, MA 02139, USA. [3]Division of Advanced Materials Engineering, Jeonbuk National University, Jeonju, South Korea. [4]Department of Materials Science and Engineering, University of Pennsylvania, Philadelphia, PA 19104, USA. [5]Department of Materials Science and Engineering, Seoul National University, Seoul, South Korea. [6]Department of Electrical Engineering and Computer Science, Massachusetts Institute of Technology, Cambridge, MA 02139, USA. [7]Center for Opto-Electronic Materials and Devices, Korea Institute of Science and Technology, Seoul, South Korea. [8]College of Computer Science, Zhejiang University, Hangzhou, China. [9]HMC, Department of Nanotechnology and Advanced Materials Engineering, Sejong University, Seoul, South Korea. [10]Department of Mechanical Engineering, Korea Advanced Institute of Science and Technology (KAIST), Daejeon, South Korea. [11]Skincare Division, Amorepacific R&D Center, Yongin, South Korea. [12]Department of Dermatology, Chung Ang University College of Medicine, Seoul, South Korea. [13]Clinical Research Lab, Skincare Division, Amorepacific R&D Center, Yongin, South Korea. [14]Department of Materials Science and Engineering, Massachusetts Institute of Technology, Cambridge, MA 02139, USA.
*Corresponding author. Email: sviviria@amorepacific.com (J.H.); jeehwan@mit.edu (J.K.)
†These authors contributed equally to this work.

properties of materials (e.g., conformability and mechanical durability), overcoming intrinsic limits of materials. Making a fractal cut between two holes forms the shape of "dumbbell." These unique dumbbell through-hole patterns construct an auxetic kirigami pattern that allows extreme conformability on the markedly bumpy surface of our skins, forming record-high work of adhesion to the skin that is comparable to commercialized skin adhesives (~20 N m^{-1}). Simultaneously, the circular holes at the edges not only act as a sweat removal paths but also suppress strain localization at the edge of the kirigami patterns, allowing fatigue-free mechanical reliability (>10^6 fatigue cycles with 2-mm bending radius; 12.5% nominal tensile strain). This aggressive patterning of the e-skin additionally allows a reduction of areal mass density to ~1.5 mg cm^{-2}, which is a near ideal value for imperceptible lamination onto the skin while maintaining excellent mechanical stability and sweat permeability. On the basis of the perforated e-skin platform, we have integrated inorganic-based temperature, hydration, strain, and ultraviolet (UV) sensor arrays that are also perforated to secure sweat-permeable channels at the active region. These perforated sensors could obtain reliable biophysical data even under profuse sweating, whereas malfunction occurred on nonperforated e-skins. With our innovations on permeability, conformability, and stability, we demonstrate daily activity checkup of skin health over a week (including exercise at the gym) with no skin irritation. This paves the way for e-skin–based long-term reliable physical health monitoring with minimized disturbance to skin homeostasis.

RESULTS

Sweat pore–inspired perforated e-skins

For full sweat permeation, we uniquely designed our e-skin by being inspired by human sweat pores. The through-hole patterns on the e-skin were constructed with the following rationales: (i) The size and interspacing of the circular holes were engineered to provide outlet of gas and sweat from sweat pores, thus allowing the skin to maintain normal physiological activities without causing e-skin delamination and sensor malfunctioning, (ii) auxetic kirigami pattern were made between two adjacent holes to reduce the Young's modulus and Poisson's ratio, thus enhancing conformality on the irregular skin surface, and (iii) circular holes at the edge of the auxetic cuts were made to relieve localized strain, thus finally constructing dumbbell shaped patterns (see Fig. 1A). Figure 1B illustrates our perforated e-skin design. Auxetic dumbbell hole patterns are integrated into all the modules that construct our e-skin, including the electronic modules [Au interconnects and polyimide (PI) encapsulation] as well as the polydimethylsiloxane (PDMS) adhesive (figs. S1 to S6 and note S1.1). To demonstrate through-hole patterns, the pattern sizes were varied at each layer considering the misalignment of each layer during e-skin fabrication (fig. S1). The e-skin contains four different physical sensors (bottom of Fig. 1B): Pt resistance thermometer, capacitive-type Au hydration sensor, ZnO thin film–based strain sensor, and ZnO UV sensor. Interdigitated electrodes of thermometers and hydration sensors follow the auxetic dumbbell hole patterns, and all electronic modules are encapsulated with a PI layer to improve mechanical robustness by placing the modules close to neutral mechanical plane (fig. S7 and note S1.2). Figure 1C shows optical images of the corresponding e-skin regions where the sensors are also perforated to secure open channels at the sensing region (see figs. S4 to S6 and note S2 for detailed information of sensors). Figures S8 to S13 show sensing characteristics of each sensor where their performances are adequate for physical health monitoring on the skin. Note that ZnO strain sensors are suspended onto through-holes (no PDMS adhesive) for enhancing the sensitivity by reducing flexural rigidity of the active region (*25*) and by suppression of strain damping in the intrinsically stretchable PDMS layer (*26*). On the other hand, ZnO UV sensors are located on the PDMS adhesives to reduce strain dependency of the device conductance, and circular hole array patterns were formed at the top PI layer to provide penetration paths of UV light and to trigger UV-induced conductance changes of ZnO.

Sweat-permeable e-skins and reliable physical sensing

We designed circular holes in our auxetic dumbbell through-hole patterns to form sweat-permeable channels, as depicted in Fig. 2A. We conservatively assumed the average outer diameter of a sweat duct and the average distance between the center of the sweat pore on human skins to be ~100 μm (*27*) and ~400 μm (*28*), respectively. On the basis of these, we fixed an interdistance of the circular holes at 200 μm to have more holes than sweat pores on the skin. Then, we simulated the percentage of fully blocked skin pores by the function of diameter of the holes, thus increasing the hole size and reducing the interspacing of the holes (right of Fig. 2A). We found that when the hole diameter is larger than 100 μm, we can form sweat-permeable channel without full blocking of skin pores. Moreover, sweat permeability can also be enhanced by adding (i) auxetic kirigami patterns and (ii) additional hole patterns, thereby maintaining physiological activities of the skin such as perspiration and suppressing sweat accumulation at the e-skin/skin interface (fig. S1). Then, we fabricated dumbbell-patterned sensor modules using conventional photolithographic processes and transferred the stack temporarily to a semitransparent thermal release tape (TRT), followed by combining PDMS patches with dumbbell holes via soft lithography (figs. S2 and S3). We first evaluated the vapor permeability of e-skins by measuring the changes of transepidermal water loss (TEWL) of the forearm after the e-skin lamination (Fig. 2B). Nonperforated e-skins show substantial reduction of TEWL by 34.63% (±6.54%). On the other hand, conventional e-skins (perforation only on electronic modules but not on elastomers) and perforated e-skins maintain 88.93% (±9.54%) and 94.54% (±7.33%) TEWL, respectively, showing their excellent vapor permeability (see fig. S14 and note S3.1 for details of TEWL changes).

Even with this excellent vapor permeability of conventional e-skin, however, actively inducing sweat on the skin does not only cause severe trapping of sweat at skin/e-skin interfaces but also induced sensor malfunctioning when the conventional e-skins were laminated to the human skin. As shown in Fig. 2C and movie S1, trapped sweat is immediately observed when laminating conventional e-skins on a forehead of our human subject right after stimulation of sweating through eating a spicy meal. On the other hand, our fully perforated e-skins maintained intimate contact without sweat accumulation at the interface. It should be noted that the demonstration of sweat permeability from our perforated e-skin is unprecedented, while vapor permeability of conventional e-skin has already been well demonstrated due to high vapor permeability of microporous silicone-based adhesives (*8*, *10*, *29*). Quantitative analysis on sweat trapped area measured by an image analyzer confirms effective evacuation of sweat from our perforated e-skin, while sweat was trapped below conventional e-skins (Fig. 2D). Although trapped sweat at the

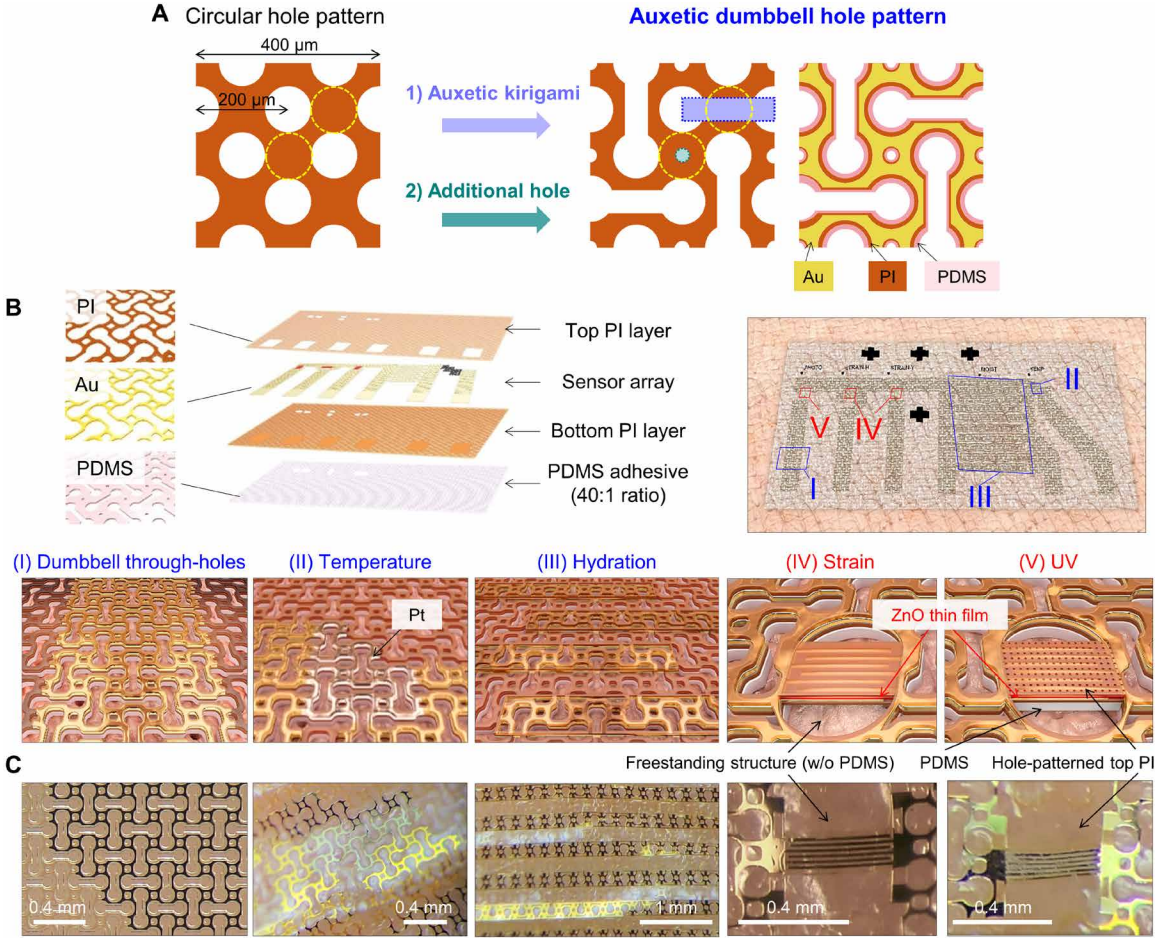

Fig. 1. Perforated e-skins with inorganic physical sensors. (**A**) Design of auxetic dumbbell through-hole patterns for driving sweat-permeable channels and synergistic physical properties of e-skins. (**B**) Schematic illustration of perforated e-skins with (I) auxetic dumbbell through-hole patterns. As the hole interspacing is narrower than the average diameter of a sweat pore, the e-skin can form open channels on the pore. Four multiple sensors—(II) Pt resistance thermometer, (III) capacitive-type Au hydration sensor, and ZnO nano–thin-film–based (IV) strain and (V) UV sensor—are also perforated to suppress sweat trapping at the sensing regions. (**C**) Optical images of the perforated e-skins showing auxetic dumbbell through-hole patterns, Pt thermometer, Au hydration sensor, ZnO strain, and UV sensor. The images were obtained after lamination on the wrist, except for the leftmost image.

conventional e-skin/skin interface disappeared owing to the high-vapor permeability, it took around 4 hours for evaporation of trapped sweat. We further verified efficient liquid dissipation through our e-skin by measuring the hydration levels on a moisturized forearm via our hydration sensor, as shown in Fig. 2E. After soaking the forearm for 5 min, the e-skin was laminated on the wet skin and the hydration level was continuously measured for 15 min. Our fully perforated e-skin (blue line) measures immediate relaxation of the actual skin hydration level, which is consistent with results estimated by a commercial hydration sensor (gray point; Corneometer CM 825), while the conventional e-skin exhibits delayed relaxation behavior (red line). Our findings prove that our perforated e-skin allows both vapor and liquid permeation, while the conventional e-skin only permits vapor exchange through the e-skin. Our e-skin's sweat permeability makes a notable impact on post-wear skin health and reliability of e-skin sensors. As shown in Fig. 2F, we monitored skin allergic reaction by a dermatologist after laminating our e-skin, conventional e-skin, and nonperforated e-skin on the forearm over a period of 1 week. Skin damages appeared for those who wore conventional/nonperforated e-skin, while none of the human subjects showed skin irritation after lamination of our perforated e-skin, thus proving excellent long-term skin compatibility of our e-skin.

In addition, we observed that our e-skin sensors reliably obtained physical information even under profuse sweating, as shown in Fig. 2G. After lamination of conventional e-skin and perforated e-skin on the forehead, we monitored movements of the forehead using the integrated strain sensors. Without sweating, both conventional and perforated e-skin correctly monitored tension and relaxation when frowning and relieving. Note that higher strain responsivity recorded from the perforated e-skin (four times) arises because a suspended freestanding structure of strain sensors reduces flexural rigidity of the sensor region (*25*), suppressing strain damping effect from the PDMS adhesive (*26*) (see note S2.1 and figs. S8 to S10 for details of the sensor performance). However, when we stimulated sweating on the forehead, sensor malfunctions occurred for conventional e-skins, while our perforated e-skin maintained its correct reading of the strain. Furthermore, as shown in Fig. 2H, sweat

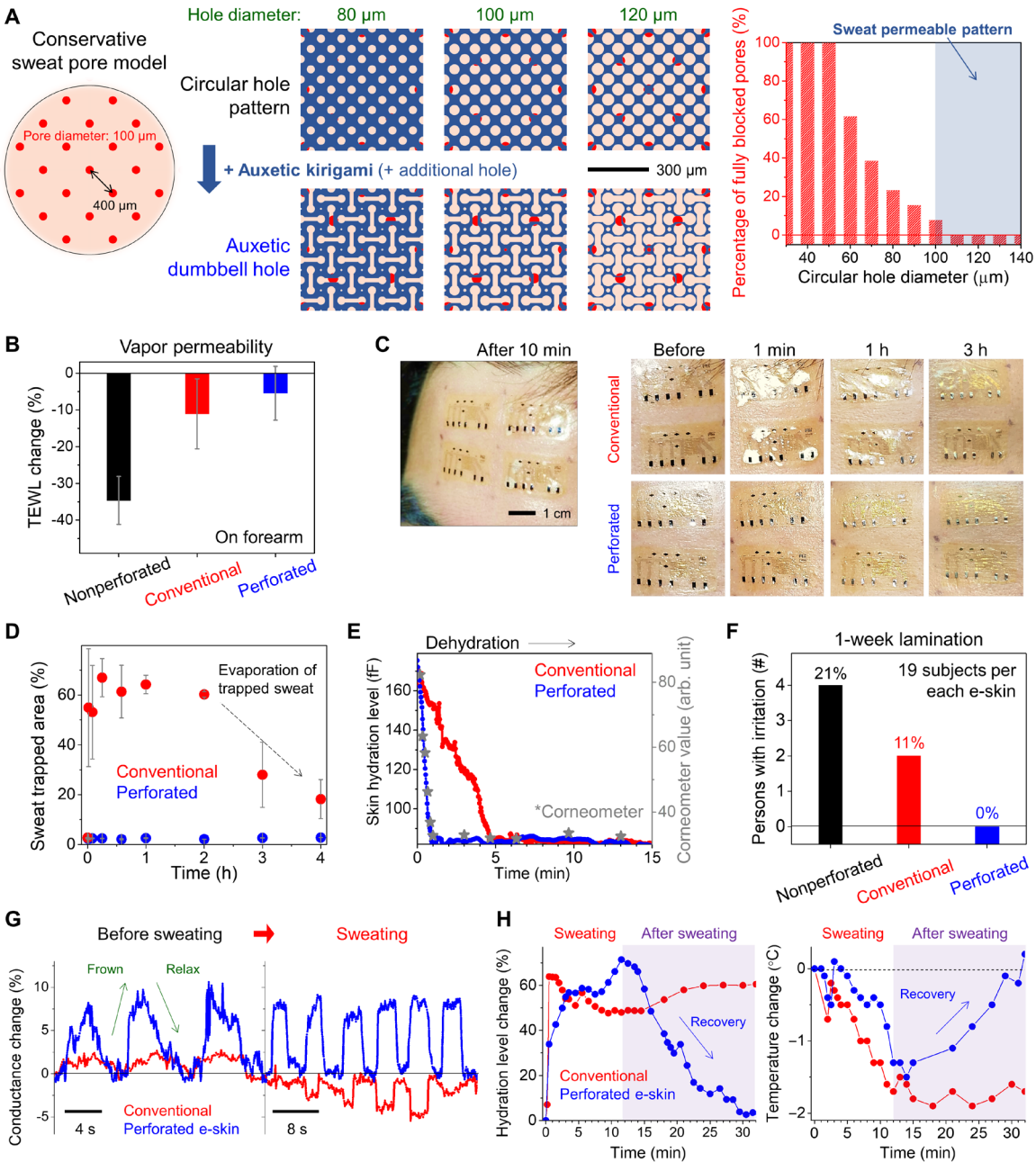

Fig. 2. Sweat-permeable e-skins with reliable physical sensing. (**A**) Precision design of auxetic dumbbell through-holes to provide open channels on sweat pores. (**B**) Changes of TEWL of the forearm after e-skin lamination. (**C**) Stability of the e-skin/forehead interface under profuse sweating (after having a spicy meal). Perforated e-skins form steady conformal contact on the forehead, whereas sweat trapping and interface delamination occurred on conventional e-skin samples. Photo credit: Hanwool Yeon, Massachusetts Institute of Technology. (**D**) Areal changes of sweat trapped region after sweating. (**E**) Dehydration monitoring of moisturized forearm. Only the fully perforated e-skin obtained similar dehydration tendencies with the reference skin region measured by commercial skin hydration analyzer (Corneometer CM 825). (**F**) Skin compatibility test of e-skins through 1-week lamination on the forearm. (**G**) Tracking of forehead movements using strain sensors. During sweating, the ZnO strain sensor in perforated e-skins reliably monitors the movement, whereas malfunction occurs at the strain sensors in conventional e-skins because of sweat trapping and interface delamination. (**H**) Changes of skin hydration level and skin temperature after profuse sweating on the forehead.

trapping at conventional e-skin/skin interface also induced wrong information from temperature and hydration sensors over 20 min, whereas the perforated e-skin could track recovery of the physical properties. These findings suggest that sweat accumulation must be avoided to achieve long-term conformability and monitorability. Our dumbbell hole patterns in the e-skin unlocked reliable operation of the e-skin for a long time, and this is achieved not only by effective dissipation of sweat but also by forming steady conformal contact on the human skin with mechanical stability, which will be further discussed in the following section.

Mechanical performance driven by auxetic dumbbell through-holes

Together with having complete evacuation of sweat, connecting two holes by line cuts forms auxetic dumbbell patterns, which have three mechanical benefits that include (i) excellent conformability due to reduced Young's modulus and Poisson's ratio with enhanced adhesion (*30*–*32*), (ii) substantial reduction of stress concentration at the tip of auxetic cuts by circular holes at the edges (although it is mainly designed for sweat dissipation) (*33*), and (iii) significant reduction of areal mass density due to largely patterned areas for long-term imperceptibility.

Figure 3A visually shows that our e-skins conformally follow the wrinkles of the skin without having significant interface delamination because of its auxetic structures (see fig. S6 for more images). We measured a record value of work of adhesion from our perforated e-skins as 20 (± 3.7) N m^{-1}, as shown in Fig. 3B, that is superior to other silicone-based e-skins (*1*) and is comparable to conventional skin bandages (*34*). It should be highlighted that although the aimed contact area of our fully perforated e-skin is smaller than that of conventional e-skin, the value of work of adhesion in our fully perforated e-skin is seven- and threefold higher than that of nonperforated e-skin and conventional e-skins, respectively (see fig. S15 for peel test results of each e-skin and note S3.2). This indicates that due to enhanced conformability of our perforated e-skins, its effective contract area is greater than that of other types of e-skins. These excellent conformability and strong work of adhesion can be attributed to skin-like nonlinear mechanical behaviors of our perforated e-skins with comparable mechanical parameters to those of the human forearm (*35*, *36*) (see fig. S16 and note S3.3 for more details). We also found that rounding of the edges of auxetic cuts in the dumbbell patterns allows excellent mechanical durability of the e-skin compared to other types of e-skins. Figure 3C shows finite element analysis (FEA) results of the tensile characteristic of three different patterns (circular hole, auxetic cut, and auxetic dumbbell). Among the patterns, our dumbbell hole patterns show efficient release of localized strain at the edges of the auxetic cuts with the lowest microscopic strain up to 30% global strain, which would prevent crack formation at the edges of the cuts (see note S3.4 and fig. S16 for further details of the results). This structural engineering leads to superior durability of the auxetic dumbbell hole–patterned e-skins against bending fatigue cyclic test compared to e-skins that only have auxetic cuts or circular hole patterns, as shown in Fig. 3 (D and E). The interconnect resistance of the e-skin with the dumbbell hole patterns was nearly unchanged during 10^6 bending fatigue

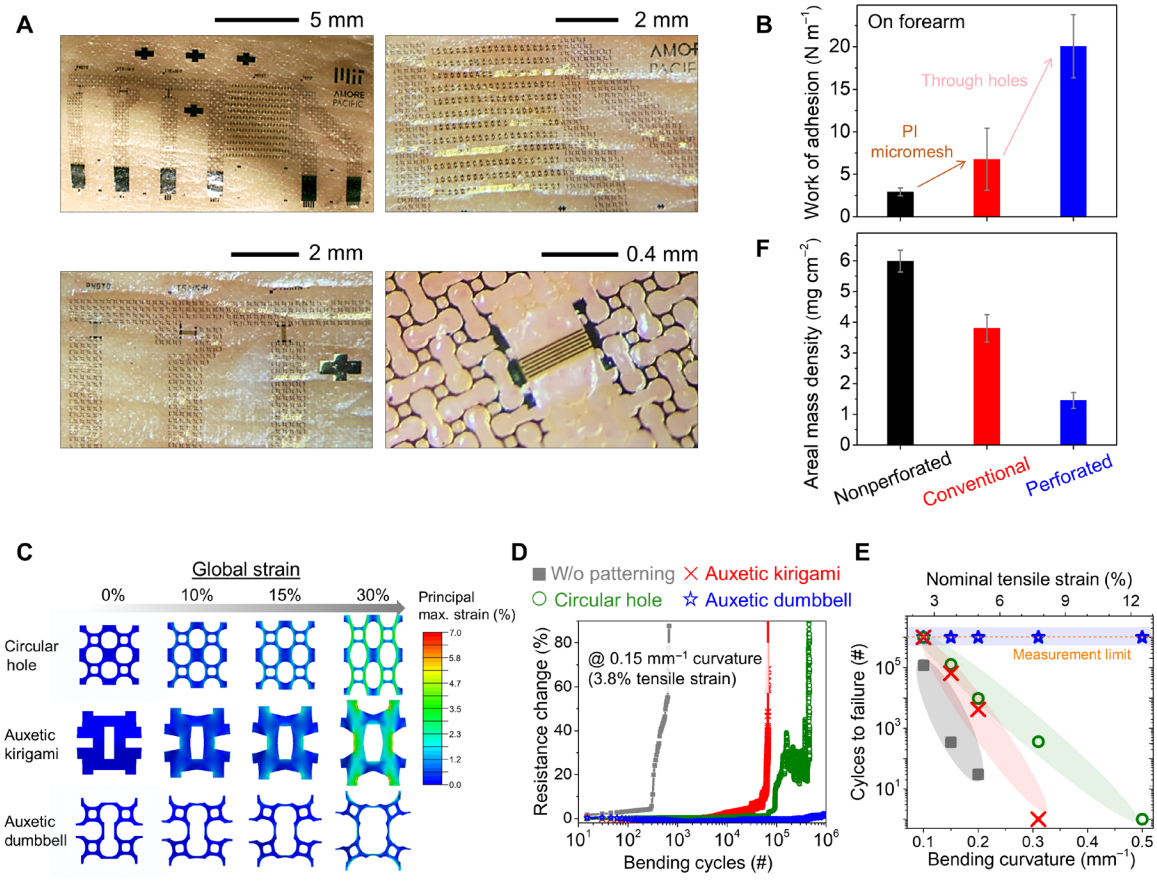

Fig. 3. Mechanical performance of perforated e-skins. (**A**) Optical images of perforated e-skins showing conformal contact on the forearm. (**B**) Work of adhesion of nonperforated, conventional, and perforated e-skins. (**C**) Strain distribution of three different patterns (circular hole, auxetic kirigami, and auxetic dumbbell) in uniaxial stretching simulation. (**D**) Cyclic bending fatigue test of e-skins under 0.15 mm^{-1} bending curvature (3.8% nominal tensile strain) with various perforated patterns (no-pattern, circular hole, auxetic kirigami, and auxetic dumbbell holes). (**E**) Mechanical durability of e-skins with respect to the bending curvature. (**F**) Areal mass density of e-skins.

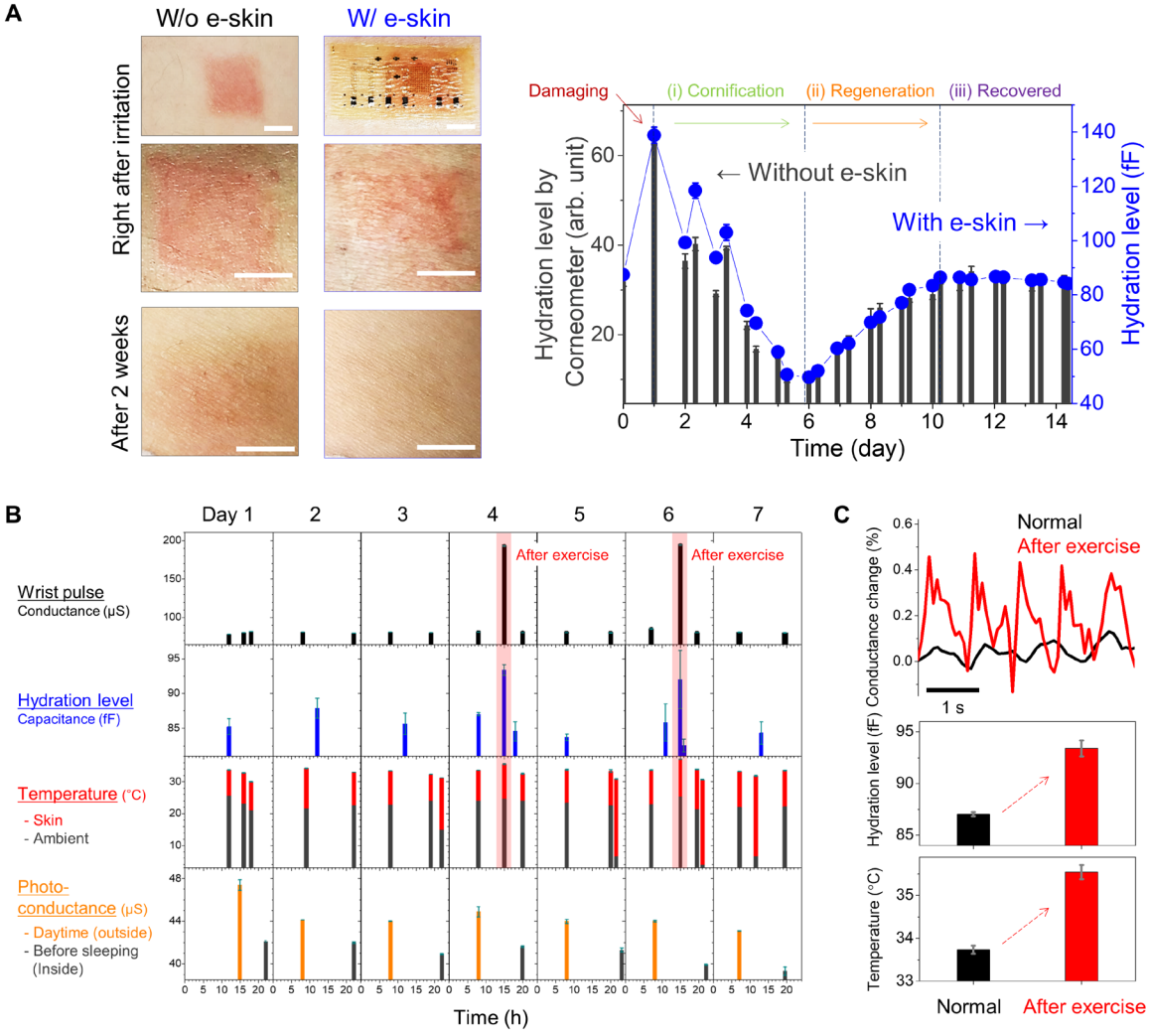

Fig. 4. Long-term health monitoring by perforated e-skins. (**A**) Skin regeneration monitoring over a period of 2 weeks. Photographs of the inflamed skin region right after erythema and after 2 weeks, showing that perforated e-skin has a negligible adverse effect to skin regeneration (left images). Scale bars, 5 mm. Hydration level of the inflamed skin as a function of e-skin lamination days (right graph). Skin hydration level was monitored by a hydration sensor in the e-skin and simultaneously compared with a conventional hydration analyzer (Corneometer CM 825). Photo credit: Haneol Lee, Massachusetts Institute of Technology. (**B**) Daily activity checkup using perforated e-skin with multiple sensors for a week: wrist pulse, skin hydration level, skin temperature, and photoconductance. (**C**) Comparison of skin information using perforated e-skin before and after exercise at the gym over 30 min (top: wrist pulse, middle: skin hydration level, and bottom: skin temperature).

cycles at 3.8% nominal tensile strain (0.15 mm^{-1} bending curvature) due to prevention of cracking at the tip, whereas other patterned e-skins failed (Fig. 3D). Although the bending strain increased to 12.5%, the dumbbell patterned interconnects survived at 10^6 cycles, while other patterned e-skins show a tendency that fatigue lifetime is inversely proportional to strain (see Fig. 3E and fig. S17 for more details). The increasing resistance with bending fatigue is mainly associated with localized strain-induced crack initiation/propagation (*37*). Thus, these results indicate that auxetic dumbbell hole design leads to fatigue-resistant e-skin by suppression of crack formation that can endure repeated mechanical deformation on skin during long-term cutaneous monitoring. Last, the auxetic dumbbell through-hole patterning substantially decreases areal mass density of e-skin of 1.45 mg cm^{-2}, only 36% of the mass density of conventional e-skins, as shown in Fig. 3F. This value is close to ideal realization of imperceptible e-skins (*1*, *8*, *19*).

Long-term seamless health monitoring

Using our e-skin with superior sweat permeability, conformability, and mechanical stability, we attempted long-term seamless monitoring of skin health over a period of a few weeks. The e-skin was never detached from the skin at any point during the monitoring period. We measured the recovery of a damaged human skin over a period of a few weeks. For connecting sensors to external power, we used a releasable connector, composed of Ga-In liquid metal and Cu wire (fig. S18A). In addition, conventional e-skins were not used to perform long-term health monitoring, as we have obtained unreliable monitoring results from the conventional e-skins even for short-term monitoring tasks. We first induced erythema on the skin by applying a sodium lauryl sulfate (SLS) solution (*38*). Then, the hydration level on the skin was constantly monitored by using hydration sensors on the perforated e-skin. Simultaneously, by using the Corneometer, we measured the hydration level on the control

area without the e-skin (Fig. 4A). The recovery of the damaged skin measured by the Corneometer shows three phases: (i) cornification due to dehydration, (ii) regeneration by returning to a normal hydration level, and (iii) recovery by maintaining a normal hydration level (see fig. S19 and note S4 for further details of the phenomena). The skin area laminated by our perforated e-skin exhibits the exact same track of skin recovery over 2 weeks as measured by the Corneometer, even while the skin is covered with the e-skin. The sensors still performed well after 2 weeks. This implies that (i) a wound healing process is not at all prohibited by our perforated e-skin due to complete interaction with the environment and (ii) the hydration sensor on our e-skin was capable of constant monitoring of the skin condition for 2 weeks without any malfunctioning, which is crucial for long-term cutaneous monitoring.

This encouraged us to operate all electronic modules for daily activity checkup for a long-term period including wrist pulse, hydration, temperature, and UV exposure by multiple sensors embedded in the perforated e-skin. Note that the releasable connects were also used for the discontinuous measurement. As shown in Fig. 4B, these parameters were successfully monitored without malfunctioning for more than a week (see fig. S18 and note S5 for the details of the demonstration including average power consumption). Because of superior reliability, our e-skin could repeatedly measure normal health information of a subject (male, 29): wrist pulse with ~51 beats per minute (bpm), skin hydration level of ~85 fF (~32 Corneometer value), and skin surface temperature of 33.7°C. Furthermore, the spatiotemporal information of the subject was obtained by the difference of photo-conductance at daytime (outside) and at nighttime (inside). On days 4 and 6, the human subject exercised (movie S2), and we were able to observe an increase in pulse, hydration, and temperature, as shown in Fig. 4C. After exercise, the blood flow was concentrated in skeletal muscles, initiating vasodilation of arterial vessels (*39*, *40*). As a result, the pulse frequency and strength were increased to 120 bpm and by a factor of 5, respectively. Furthermore, skin temperature increased from 33.7° to 35.6°C and perspiration increased the skin hydration level. This unprecedented demonstration of long-term monitoring with multiple e-skin sensors offers advanced e-skin platforms for long-term, noninvasive health monitoring.

DISCUSSION

We have demonstrated simple and novel approaches to form long-term stable conformal skin-interfaced system. Our auxetic dumbbell through-hole patterns simultaneously enhance physical properties of conventional e-skin platform including mechanical reliability, conformability, work of adhesion, and areal mass density. The through-hole patterns, of which design is inspired from sweat pores, provide sweat-permeable channels and secure the skin homeostasis as well as conformal interface for a long-term period. In addition, perforation-engineered inorganic physical sensors reliably obtained health information from the skin even under profuse sweating because of the steady conformal interface. Although our perforated e-skins should be advanced in terms of real-time monitorability, long-term health monitoring tests were successfully performed including tracking of skin regeneration with no disturbance and daily activity checkup over a period of 1 week. We believe that our perforating design rules can open new directions for implementing reliable e-skin sensors for long-term health monitoring applications.

MATERIALS AND METHODS

Fabrication of electronic modules for perforated e-skins

Figure S2 illustrates the fabrication processes. Electronic modules were fabricated on Al/Ti (200 nm/40 nm)–coated, conductive Si wafer (<0.01 ohm·cm) and were released from the wafer through electrochemical dissolution of the Al layer. As a first step, the bottom PI layer (2 μm) was formed on the Al/Ti/Si wafer by spin coating and curing process (250°C for 1 hour). Au interconnects (100 nm) with the Cr adhesive layer (1 nm) were deposited on the bottom PI by e-beam evaporation and were patterned by the photoresist-based lift-off process (LOR 3A, MicroChem). For temperature sensor formation, auxetic Pt dumbbell meshes (40 nm) were formed between Au interconnects by e-beam evaporation and the subsequent lift-off process. For formation of ZnO thin-film sensors, ZnO thin films (100 nm) were directly deposited to Au contact/interconnects on the bottom PI by radio frequency (RF) sputtering at 200°C and were patterned using HCl solution. The HfO_2 layer (1.5 nm thick) was inserted at ZnO/Au contact by the atomic layer deposition process at 225°C, resulting in Schottky barrier formation (see fig. S8, B and D). Furthermore, the HfO_2 capping layer (3 nm) was formed at the ZnO top surface for the protection from subsequent processes. The top PI layer (2 μm) was formed on the entire sample surface to locate the electronic circuits near neutral mechanical plane, thereby improving the mechanical robustness (note S1.2 and fig. S7). Note that some interfaces among layers were treated with 1% (v/v) 3-aminopropyltriethoxysilane (APTES) in deionized water to improve interface strength. Last, after the PI layers are patterned by oxygen plasma with a Cu hard mask (50 nm), fabrication of the auxetic dumbbell hole–patterned electronic modules is completed.

Perforated e-skin fabrication

For integration of the electronic modules to the auxetic dumbbell hole–patterned PDMS adhesives (SYLGARD 184, Dow Corning), detachment of the electronic modules by the electrochemical lift-off process (dissolution of Al sacrificial layer) was the first step, as shown in fig. S2. Before the lift-off process, the electronic modules were attached to TRT. Between modules and TRT, the 2-μm-thick poly(methyl methacrylate) (PMMA) layer was inserted. After electrical wiring at the backside of the Si substrate, the samples were dipped into NaCl solution (0.9% NaCl) together with Pt wire as a counter electrode. As 3 V was applied to the Si wafer, the Al was dissolved in NaCl solution and electronic modules were transferred to the TRT accordingly. To form auxetic dumbbell through-hole patterns in the electronic modules and the PDMS adhesives, Si mold–based soft lithography processes were used as illustrated in fig. S3. First, dumbbell-shaped Si mold (~20 μm depth) was prepared by deep reactive ion etching (DRIE). After spin coating of off-stoichiometric, sticky PDMS gels (40:1 weight ratio of PDMS prepolymer:curing agent) on the Si mold, the electronic modules with TRT were placed on the uncured PDMS. Semitransparency of the TRT allowed us to align auxetic dumbbell mesh of the electronic circuits with the Si mold. After the alignment, the PDMS layer was cured at 80°C with a constant pressure (1.29 kPa) to maximize the yield of the through-hole formation in e-skin. Note that a weight (1 kg) was used to apply the pressure where a flat steel plat was inserted between a weight and an e-skin sample on Si mold for spatially uniform through-holes. After PDMS curing, the Si mold was separated from the samples. Note that the Si mold was treated with trichloro(1*H*, 1*H*, 2*H*, 2*H*-perfluorooctyl)silane to reduce the Si

surface energy, while APTES treatment was conducted on the surface of the electronic modules right before placing onto the uncured PDMS adhesives. Thus, the interface strength between the electronic modules and the PDMS adhesive is much stronger than Si mold/PDMS interface strength, and these interface engineering processes facilitated the transfer of PDMS adhesives to the electronic modules without notable damages. For spatially uniform coating of the silane, oxygen plasma treatment is necessary to form hydrophilic Si mold surface. After detachment of the perforated electronic modules and the perforated PDMS adhesives from the Si mold, the TRT was released by heating at 150°C and the samples were dipped into acetone to remove PMMA. As the PMMA layer was dissolved, the perforated e-skin is produced. The perforated e-skin was scooped from acetone using cellulose wipers (TX2009, Texwipe) and cleaned by isopropanol. After drying of the perforated e-skin on the wipers, the edge of the perforated e-skin was attached to a temporary tattoo paper (Silhouette, USA), which acts as a temporary handling layer (fig. S5A). Note that the PDMS adhesion can be degraded when the e-skin samples are exposed to air for over 2 weeks. This environmental aging is strongly related with interaction of PDMS surface with air (moisture and oxygen) *(34)*. To suppress the environmental aging effect, all experiments were performed only when e-skin samples were exposed to air less than a week.

Finite element simulation

FEA was performed with ABAQUS/CAE. Three representative volume element (RVE) models, circular hole, auxetic kirigami, and dumbbell hole pattern were prepared with computer-aided design software. A periodic boundary condition was applied to the individual RVE model to reduce computation costs. C3D8 mesh elements were used. Before the stretch simulation, linear buckling analysis determined buckling eigenmodes. The resultant modes served as initial imperfection of individual model for post-buckling calculation. To observe the tensile behavior of each geometry, displacement was applied at both ends so that the global strain reached 30%. Linear elastic property was used for PI material (2.5 GPa Young's modulus, 0.3 Poisson's ratio).

Evaluation of mechanical properties and reliability

Uniaxial tensile tests were conducted with a micro material tester (MMT-500N, Shimadzu, Japan), and the electrical resistance of interconnects on the e-skin was measured simultaneously (*41*). The strain rate was 5% min^{-1}. For bending fatigue test, various types of Au interconnects (unpatterned, circular hole, auxetic kirigami, and auxetic dumbbell hole patterns) were formed on the e-skin (fig. S17). To load the samples into a sliding bending fatigue tester (Slide tester, CKSI, South Korea), each sample was attached on a 125-μm-thick PI handling substrate. The width and length of each sample were 4 mm and 20 mm, respectively. The fatigue system consists of two plates (fig. S17A): The top plate is stationary, while the bottom plate moves in a cyclic linear motion (*37*). The e-skin/PI substrates were bent between two plates, and a cyclic strain was applied on the e-skin samples as the bottom plate was displaced repeatedly. Because the e-skin samples were positioned outward from the PI handling substrate, tensile strain was applied upon bending. The linear displacement of the bottom plate was 10 mm, and the maximum cycling number was 10^6 with 5-Hz cycling frequency. The bending radius condition was modulated from 10.8 mm (2.3% nominal tensile strain) to 2 mm (12.5% tensile strain). See fig. S7C and notes S1.2 and S3.4 for details of calculation of the nominal bending strain. During the bending fatigue test, electrical resistance of the Au interconnects on e-skin was measured simultaneously using Agilent 34410A to monitor the evolution of fatigue damages on the Au interconnects.

Peel test

Adhesion force of the e-skin was evaluated by a peel test, which was executed by a customized loading machine with a translational stage and a load cell for accurate control of the moving speed (*42*). Before measurements, the e-skin was conformably laminated onto the human forearm. One end of the laminated e-skin was grabbed and fixed to the load cell. For peeling the e-skin from the skin, the load cell and the translational stage simultaneously shifted in the z and x direction with a speed of 0.2 mm s^{-1}, respectively.

Sensor assessment

Capacitance-voltage (*C-V*) and capacitance-time (*C-t*) measurements of the skin hydration sensor were carried out with an Agilent B1500A semiconductor device parameter analyzer. Changes of the electrical conductance of the temperature sensor, the strain sensor, and the UV sensor were monitored by current-voltage (*I-V*) and current-time (*I-t*) mode of Keithley 2400 Sourcemeter. Portable National Instruments USB-4067 6 ½ Digit DMM was also used to collect the electrical resistance data from the temperature sensor.

Evaluation of UV-sensing performance

UV conformal photocurrent microscopy (UVCPM) system was established to assess UV-sensing performance of ZnO e-skin sensors (see note S2.3 and fig. S12 for details of UVCPM system). The output currents from sensors were recorded with varying biases and illumination intensity with an Agilent B1500A semiconductor device parameter analyzer.

E-skin conformability and sensing reliability under profuse sweating

After the e-skin lamination onto the forehead, sweating was stimulated by eating a spicy meal. The sweating-induced changes of the e-skin conformability and sensing accuracy of the e-skin sensors were assessed simultaneously. The test was approved by Massachusetts Institute of Technology, Committee on the Use of Humans as Experimental Subjects (approval number: 1706011631R002).

Skin assessment after 1-week e-skin lamination

Nineteen human subjects executed e-skin lamination tests (4 male and 15 female subjects, average age of 31.3). Subjects attached the e-skins (nonperforated, conventional, and perforated e-skins) onto the forearm, which was preserved by a rubber-based air-permeable protector from external mechanical stresses. After 1 week, the e-skins were removed from the subject's arm. Skin health evaluation of visual comparison (Visia-CR, Canfield) was conducted before e-skin attachment and immediately, 1 hour, and 24 hours after e-skin removal, each two times. In visual comparison, visible symptoms (e.g., erythema, edema, dryness, and scales) of subjects were evaluated from one to four points, and conscious symptoms (e.g., tingling, burning, and itching) of subjects were recorded to the case reports. On the basis of meticulous evaluation, the safety of the e-skin was judged. The test was approved by AMORE PACIFIC, Institutional Review Board Committee (approval number: 2019-1SR-N088S).

Skin regeneration test for 2 weeks

First, two regions of the forearm were intentionally irritated by application of 35 μl of 1% SLS solution for 24 hours (*36*). One of the inflamed skin regions was covered by our perforated e-skin, and the other region was exposed to the ambient (controlled region). For 2 weeks, the degree of skin regeneration was estimated by measuring the skin hydration level using a hydration sensor of the e-skin and/or commercial hydration analyzer (Corneometer CM 825) on the control region. The test was approved by Massachusetts Institute of Technology, Committee on the Use of Humans as Experimental Subjects (approval number: 2003000116).

Daily activity checkup for 1 week

Perforated e-skin with multiple sensors including strain, UV, temperature, and hydration sensors was laminated onto the human wrist. To obtain health information from the e-skin over a long period, releasable interconnects, composed of Ga-In eutectic liquid metal and Cu wires, were used. In addition, the e-skin was passivated from mechanical frictions caused by clothing using a patch test chamber (The Hill Top Chamber, Cliantha Research). Note S5 and fig. S18 contain details of the experiment. The test was approved by Massachusetts Institute of Technology, Committee on the Use of Humans as Experimental Subjects (approval number: 1706011631R002).

SUPPLEMENTARY MATERIALS

Supplementary material for this article is available at http://advances.sciencemag.org/cgi/content/full/7/27/eabg8459/DC1

REFERENCES AND NOTES

1. D.-H. Kim, N. Lu, R. Ma, Y.-S. Kim, R.-H. Kim, S. Wang, J. Wu, S. M. Won, H. Tao, A. Islam, K. J. Yu, T. Kim, R. Chowdhury, M. Ying, L. Xu, M. Li, H.-J. Chung, H. Keum, M. McCormick, P. Liu, Y.-W. Zhang, F. G. Omenetto, Y. Huang, T. Coleman, J. A. Rogers, Epidermal electronics. *Science* **333**, 838–843 (2011).
2. S. Xu, A. Jayaraman, J. A. Rogers, Skin sensors are the future of health care. *Nature* **571**, 319–321 (2019).
3. T. Someya, M. Amagai, Toward a new generation of smart skins. *Nat. Biotechnol.* **37**, 382–388 (2019).
4. D.-H. Kim, J.-H. Ahn, W. M. Choi, H.-S. Kim, T.-H. Kim, J. Song, Y. Y. Huang, Z. Liu, C. Lu, J. A. Rogers, Stretchable and foldable silicon integrated circuits. *Science* **320**, 507–511 (2008).
5. J. Kim, M. Lee, H. J. Shim, R. Ghaffari, H. R. Cho, D. Son, Y. H. Jung, M. Soh, C. Choi, S. Jung, K. Chu, D. Jeon, S.-T. Lee, J. H. Kim, S. H. Choi, T. Hyeon, D.-H. Kim, Stretchable silicon nanoribbon electronics for skin prosthesis. *Nat. Commun.* **5**, 5747 (2014).
6. K. Sim, Z. Rao, Z. Zou, F. Ershad, J. Lei, A. Thukral, J. Chen, Q.-A. Huang, J. Xiao, C. Yu, Metal oxide semiconductor nanomembrane–based soft unnoticeable multifunctional electronics for wearable human-machine interfaces. *Sci. Adv.* **5**, eav9653 (2019).
7. J. A. Rogers, T. Someya, Y. Huang, Materials and mechanics for stretchable electronics. *Science* **327**, 1603–1607 (2010).
8. K.-I. Jang, S. Y. Han, S. Xu, K. E. Mathewson, Y. Zhang, J.-W. Jeong, G.-T. Kim, R. C. Webb, J. W. Lee, T. J. Dawidczyk, R. H. Kim, Y. M. Song, W.-H. Yeo, S. Kim, H. Cheng, S. Il Rhee, J. Chung, B. Kim, H. U. Chung, D. Lee, Y. Yang, M. Cho, J. G. Gaspar, R. Carbonari, M. Fabiani, G. Gratton, Y. Huang, J. A. Rogers, Rugged and breathable forms of stretchable electronics with adherent composite substrates for transcutaneous monitoring. *Nat. Commun.* **5**, 4779 (2014).
9. M. K. Choi, O. K. Park, C. Choi, S. Qiao, R. Ghaffari, J. Kim, D. J. Lee, M. Kim, W. Hyun, S. J. Kim, H. J. Hwang, S.-H. Kwon, T. Hyeon, N. Lu, D.-H. Kim, Cephalopod-inspired miniaturized suction cups for smart medical skin. *Adv. Healthc. Mater.* **5**, 80–87 (2016).
10. L. Tian, B. Zimmerman, A. Akhtar, K. J. Yu, M. Moore, J. Wu, R. J. Larsen, J. W. Lee, J. Li, Y. Liu, B. Metzger, S. Qu, X. Guo, K. E. Mathewson, J. A. Fan, J. Cornman, M. Fatina, Z. Xie, Y. Ma, J. Zhang, Y. Zhang, F. Dolcos, M. Fabiani, G. Gratton, T. Bretl, L. J. Hargrove, P. V. Braun, Y. Huang, J. A. Rogers, Publisher Correction: Large-area MRI-compatible epidermal electronic interfaces for prosthetic control and cognitive monitosring. *Nat. Biomed. Eng.* **3**, 415 (2019).
11. R. C. Webb, A. P. Bonifas, A. Behnaz, Y. Zhang, K. J. Yu, H. Cheng, M. Shi, Z. Bian, Z. Liu, Y.-S. Kim, W.-H. Yeo, J. S. Park, J. Song, Y. Li, Y. Huang, A. M. Gorbach, J. A. Rogers, Ultrathin conformal devices for precise and continuous thermal characterization of human skin. *Nat. Mater.* **12**, 938–944 (2013).
12. C. Dagdeviren, Y. Shi, P. Joe, R. Ghaffari, G. Balooch, K. Usgaonkar, O. Gur, P. L. Tran, J. R. Crosby, M. Meyer, Y. Su, R. Chad Webb, A. S. Tedesco, M. J. Slepian, Y. Huang, J. A. Rogers, Conformal piezoelectric systems for clinical and experimental characterization of soft tissue biomechanics. *Nat. Mater.* **14**, 728–736 (2015).
13. W. Gao, S. Emaminejad, H. Y. Y. Nyein, S. Challa, K. Chen, A. Peck, H. M. Fahad, H. Ota, H. Shiraki, D. Kiriya, D. H. Lien, G. A. Brooks, R. W. Davis, A. Javey, Fully integrated wearable sensor arrays for multiplexed in situ perspiration analysis. *Nature* **529**, 509–514 (2016).
14. Y. Yang, Y. Song, X. Bo, J. Min, O. S. Pak, L. Zhu, M. Wang, J. Tu, A. Kogan, H. Zhang, T. K. Hsiai, Z. Li, W. Gao, A laser-engraved wearable sensor for sensitive detection of uric acid and tyrosine in sweat. *Nat. Biotechnol.* **38**, 217–224 (2020).
15. Y. Yu, J. Nassar, C. Xu, J. Min, Y. Yang, A. Dai, R. Doshi, A. Huang, Y. Song, R. Gehlhar, A. D. Ames, W. Gao, Biofuel-powered soft electronic skin with multiplexed and wireless sensing for human-machine interfaces. *Sci. Robot.* **5**, eaaz7946 (2020).
16. A. J. Bandodkar, S. P. Lee, I. Huang, W. Li, S. Wang, C.-J. Su, W. J. Jeang, T. Hang, S. Mehta, N. Nyberg, P. Gutruf, J. Choi, J. Koo, J. T. Reeder, R. Tseng, R. Ghaffari, J. A. Rogers, Sweat-activated biocompatible batteries for epidermal electronic and microfluidic systems. *Nat. Electron.* **3**, 554–562 (2020).
17. D. Y. M. Leung, A. Calatroni, L. S. Zaramela, P. K. LeBeau, N. Dyjack, K. Brar, G. David, K. Johnson, S. Leung, M. Ramirez-Gama, B. Liang, C. Rios, M. T. Montgomery, B. N. Richers, C. F. Hall, K. A. Norquest, J. Jung, I. Bronova, S. Kreimer, C. Conover Talbot, D. Crumrine, R. N. Cole, P. Elias, K. Zengler, M. A. Seibold, E. Berdyshev, E. Goleva, The nonlesional skin surface distinguishes atopic dermatitis with food allergy as a unique endotype. *Sci. Transl. Med.* **11**, eaav2685 (2019).
18. H. U. Chung, B. H. Kim, J. Y. Lee, J. Lee, Z. Xie, E. M. Ibler, K. H. Lee, A. Banks, J. Y. Jeong, J. Kim, C. Ogle, D. Grande, Y. Yu, H. Jang, P. Assem, D. Ryu, J. W. Kwak, M. Namkoong, J. B. Park, Y. Lee, D. H. Kim, A. Ryu, J. Jeong, K. You, B. Ji, Z. Liu, Q. Huo, X. Feng, Y. Deng, Y. Xu, K. I. Jang, J. Kim, Y. Zhang, R. Ghaffari, C. M. Rand, M. Schau, A. Hamvas, D. E. Weese-Mayer, Y. Huang, S. M. Lee, C. H. Lee, N. R. Shanbhag, A. S. Paller, S. Xu, J. A. Rogers, Binodal, wireless epidermal electronic systems with in-sensor analytics for neonatal intensive care. *Science* **363**, eaau0780 (2019).
19. A. Miyamoto, S. Lee, N. F. Cooray, S. Lee, M. Mori, N. Matsuhisa, H. Jin, L. Yoda, T. Yokota, A. Itoh, M. Sekino, H. Kawasaki, T. Ebihara, M. Amagai, T. Someya, Inflammation-free, gas-permeable, lightweight, stretchable on-skin electronics with nanomeshes. *Nat. Nanotechnol.* **12**, 907–913 (2017).
20. X. Peng, K. Dong, C. Ye, Y. Jiang, S. Zhai, R. Cheng, D. Liu, X. Gao, J. Wang, Z. L. Wang, A breathable, biodegradable, antibacterial, and self-powered electronic skin based on all-nanofiber triboelectric nanogenerators. *Sci. Adv.* **6**, eaba9624 (2020).
21. M. O. G. Nayeem, S. Lee, H. Jin, N. Matsuhisa, H. Jinno, A. Miyamoto, T. Yokota, T. Someya, All-nanofiber-based, ultrasensitive, gas-permeable mechanoacoustic sensors for continuous long-term heart monitoring. *Proc. Natl. Acad. Sci. U.S.A.* **117**, 7063–7070 (2020).
22. Y. J. Fan, X. Li, S. Y. Kuang, L. Zhang, Y. H. Chen, L. Liu, K. Zhang, S. W. Ma, F. Liang, T. Wu, Z. L. Wang, G. Zhu, Highly robust, transparent, and breathable epidermal electrode. *ACS Nano* **12**, 9326–9332 (2018).
23. W. Zhou, S. Yao, H. Wang, Q. Du, Y. Ma, Y. Zhu, Gas-permeable, ultrathin, stretchable epidermal electronics with porous electrodes. *ACS Nano* **14**, 5798–5805 (2020).
24. J. Lewis, Material challenge for flexible organic devices. *Mater. Today* **9**, 38–45 (2006).
25. L. Beker, N. Matsuhisa, I. You, S. R. A. Ruth, S. Niu, A. Foudeh, J. B.-H. Tok, X. Chen, Z. Bao, A bioinspired stretchable membrane-based compliance sensor. *Proc. Natl. Acad. Sci. U.S.A.* **117**, 11314–11320 (2020).
26. D. Son, J. Lee, S. Qiao, R. Ghaffari, J. Kim, J. E. Lee, C. Song, S. J. Kim, D. J. Lee, S. W. Jun, S. Yang, M. Park, J. Shin, K. Do, M. Lee, K. Kang, C. S. Hwang, N. Lu, T. Hyeon, D.-H. Kim, Multifunctional wearable devices for diagnosis and therapy of movement disorders. *Nat. Nanotechnol.* **9**, 397–404 (2014).
27. Z. Sonner, E. Wilder, J. Heikenfeld, G. Kasting, F. Beyette, D. Swaile, F. Sherman, J. Joyce, J. Hagen, N. Kelley-Loughnane, R. Naik, The microfluidics of the eccrine sweat gland, including biomarker partitioning, transport, and biosensing implications. *Biomicrofluidics* **9**, 031301 (2015).
28. N. A. Taylor, C. A. Machado-Moreira, Regional variations in transepidermal water loss, eccrine sweat gland density, sweat secretion rates and electrolyte composition in resting and exercising humans. *Extrem. Physiol. Med.* **2**, 4 (2013).
29. A. Lamberti, S. L. Marasso, M. Cocuzza, PDMS membranes with tunable gas permeability for microfluidic applications. *RSC Adv.* **4**, 61415–61419 (2014).
30. Y. Cho, J.-H. Shin, A. Costa, T. A. Kim, V. Kunin, J. Li, S. Y. Lee, S. Yang, H. N. Han, I.-S. Choi, D. J. Srolovitz, Engineering the shape and structure of materials by fractal cut. *Proc. Natl. Acad. Sci. U.S.A.* **111**, 17390–17395 (2014).
31. K.-B. Kim, Y.-J. Lee, A. Costa, Y.-K. Lee, T.-S. Jang, M.-G. Lee, Y.-C. Joo, K. H. Oh, J. Song, I.-S. Choi, Extremely versatile deformability beyond materiality: A new material platform through simple cutting for rugged batteries. *Adv. Eng. Mater.* **21**, 1900206 (2019).
32. Y.-K. Lee, Z. Xi, Y.-J. Lee, Y.-H. Kim, Y. Hao, H. Choi, M.-G. Lee, Y.-C. Joo, C. Kim, J.-M. Lien, I.-S. Choi, Computational wrapping: A universal method to wrap 3D-curved surfaces with nonstretchable materials for conformal devices. *Sci. Adv.* **6**, eax6212 (2020).

33. B.-J. Kim, Y. Cho, M.-S. Jung, H.-A.-S. Shin, M.-W. Moon, H. N. Han, K. T. Nam, Y.-C. Joo, I.-S. Choi, Fatigue-free, electrically reliable copper electrode with nanohole array. *Small* **8**, 3300–3306 (2012).
34. L. Liu, K. Kuffel, D. K. Scott, G. Constantinescu, H.-J. Chung, J. Rieger, Silicone-based adhesives for long-term skin application: Cleaning protocols and their effect on peel strength. *Biomed. Phys. Eng. Express.* **4**, 15004 (2018).
35. K.-I. Jang, H. U. Chung, S. Xu, C. H. Lee, H. Luan, J. Jeong, H. Cheng, G.-T. Kim, S. Y. Han, J. W. Lee, J. Kim, M. Cho, F. Miao, Y. Yang, H. N. Jung, M. Flavin, H. Liu, G. W. Kong, K. J. Yu, S. Il Rhee, J. Chung, B. Kim, J. W. Kwak, M. H. Yun, J. Y. Kim, Y. M. Song, U. Paik, Y. Zhang, Y. Huang, J. A. Rogers, Soft network composite materials with deterministic and bio-inspired designs. *Nat. Commun.* **6**, 6566 (2015).
36. Y. Ma, X. Feng, J. A. Rogers, Y. Huang, Y. Zhang, Design and application of 'J-shaped' stress–strain behavior in stretchable electronics: A review. *Lab Chip* **17**, 1689–1704 (2017).
37. B.-J. Kim, H.-A.-S. Shin, S.-Y. Jung, Y. Cho, O. Kraft, I.-S. Choi, Y.-C. Joo, Crack nucleation during mechanical fatigue in thin metal films on flexible substrates. *Acta Mater.* **61**, 3473–3481 (2013).
38. L. J. Petersen, A. M. Lyngholm, L. Arendt-Nielsen, A novel model of inflammatory pain in human skin involving topical application of sodium lauryl sulfate. *Inflamm. Res.* **59**, 775–781 (2010).
39. R. B. Armstrong, M. H. Laughlin, Blood flows within and among rat muscles as a function of time during high speed treadmill exercise. *J. Physiol.* **344**, 189–208 (1983).
40. I. Sarelius, U. Pohl, Control of muscle blood flow during exercise: Local factors and integrative mechanisms. *Acta Physiol.* **199**, 349–365 (2010).
41. Y.-Y. Lee, J.-H. Lee, J.-Y. Cho, N.-R. Kim, D.-H. Nam, I.-S. Choi, K. T. Nam, Y.-C. Joo, Stretching-induced growth of PEDOT-rich cores: A new mechanism for strain-dependent resistivity change in PEDOT:PSS Films. *Adv. Funct. Mater.* **23**, 4020–4027 (2013).
42. J. Seo, C. Kim, B. S. Ma, T.-I. Lee, J. H. Bong, J. G. Oh, B. J. Cho, T.-S. Kim, Direct graphene transfer and its application to transfer printing using mechanically controlled, large area graphene/copper freestanding layer. *Adv. Funct. Mater.* **28**, 1707102 (2018).
43. Y. Zhang, Y. Liu, Z. L. Wang, Fundamental theory of piezotronics. *Adv. Mater.* **23**, 3004–3013 (2011).
44. X. Wen, W. Wu, Y. Ding, Z. L. Wang, Piezotronic effect in flexible thin-film based devices. *Adv. Mater.* **25**, 3371–3379 (2013).
45. W. Wu, Z. L. Wang, Piezotronics and piezo-phototronics for adaptive electronics and optoelectronics. *Nat. Rev. Mater.* **1**, 16031 (2016).
46. Sandia National Laboratories, United States Department of Energy, Office of Scientific and Technical Information, *Work Functions of the Transition Metals and Metal Silicides* (United States Department of Energy, 1999).
47. K. Jacobi, G. Zwicker, A. Gutmann, Work function, electron affinity and band bending of zinc oxide surfaces. *Surf. Sci.* **141**, 109–125 (1984).
48. L. J. Brillson, Y. Lu, ZnO Schottky barriers and ohmic contacts. *J. Appl. Phys.* **109**, 121301 (2011).
49. T. A. Krajewski, G. Luka, S. Gieraltowska, A. J. Zakrzewski, P. S. Smertenko, P. Kruszewski, L. Wachnicki, B. S. Witkowski, E. Lusakowska, R. Jakiela, M. Godlewski, E. Guziewicz, Hafnium dioxide as a passivating layer and diffusive barrier in ZnO/Ag Schottky junctions obtained by atomic layer deposition. *Appl. Phys. Lett.* **98**, 263502 (2011).
50. A. O. Barel, P. Clarys, In vitro calibration of the capacitance method (Corneometer CM 825) and conductance method (Skicon-200) for the evaluation of the hydration state of the skin. *Skin Res. Technol.* **3**, 107–113 (1997).
51. D. J. Lichtenwalner, A. E. Hydrick, A. I. Kingon, Flexible thin film temperature and strain sensor array utilizing a novel sensing concept. *Sens. Actuat. A Phys.* **135**, 593–597 (2007).
52. A. Janotti, C. G. Van de Walle, Fundamentals of zinc oxide as a semiconductor. *Rep. Prog. Phys.* **72**, 126501 (2009).
53. Q. Hua, J. Sun, H. Liu, R. Bao, R. Yu, J. Zhai, C. Pan, Z. L. Wang, Skin-inspired highly stretchable and conformable matrix networks for multifunctional sensing. *Nat. Commun.* **9**, 244 (2018).
54. D. H. Zhang, Fast photoresponse and the related change of crystallite barriers for ZnO films deposited by RF sputtering. *J. Phys. D Appl. Phys.* **28**, 1273–1277 (1995).
55. P. Sharma, K. Sreenivas, K. V. Rao, Analysis of ultraviolet photoconductivity in ZnO films prepared by unbalanced magnetron sputtering. *J. Appl. Phys.* **93**, 3963–3970 (2003).
56. V. Arumugam, M. D. Naresh, R. Sanjeevi, Effect of strain rate on the fracture behaviour of skin. *J. Biosci.* **19**, 307–313 (1994).
57. D. Y. W. Yu, F. Spaepen, The yield strength of thin copper films on Kapton. *J. Appl. Phys.* **95**, 2991–2997 (2004).
58. T. Agner, J. Serup, Skin reactions to irritants assessed by non-invasive bioengineering methods. *Contact Dermatitis* **20**, 352–359 (1989).
59. J. L. Lévêque, J. de Rigal, D. Saint-Léger, D. Billy, How does sodium lauryl sulfate alter the skin barrier function in man? A multiparametric approach. *Skin Pharmacol. Physiol.* **6**, 111–115 (1993).
60. H. Tagami, H. Kobayashi, X.-S. Zhen, K. Kikuchi, Environmental effects on the functions of the stratum corneum. *J. Investig. Dermatol. Symp. Proc.* **6**, 87–94 (2001).
61. J. M. Johnson, L. B. Rowell, G. L. Brengelmann, Modification of the skin blood flow-body temperature relationship by upright exercise. *J. Appl. Physiol.* **37**, 880–886 (1974).
62. D. M. DiPasquale, M. J. Buono, F. W. Kolkhorst, Effect of skin temperature on the cholinergic sensitivity of the human eccrine sweat gland. *Jpn. J. Physiol.* **53**, 427–430 (2003).

Acknowledgments

Funding: This work is supported by AMOREPACIFIC. **Author contributions:** H.Y., J.H., and J.K. conceived this work, and J.K. supervised the team. H.Y., H.L., and J.K. designed experiments and prepared the manuscript. H.Y. and H.L. developed perforated e-skins. H.Y., H.L., and D.L. performed the device fabrication. Y.K., J.S., J.K., J.M.S., J.L., S.K., S.H., and S.-H.B. contributed to equipment setup for e-skin fabrication. P.L., C.C., and J.L. made measurement programs. H.Y., H.L., C.C., D.L., H.K., J.K., D.K., K.K., H.S.K., and M.-C.P. performed the e-skin sensor measurement and image analysis of e-skins. H.L. and H.Y. conducted long-term health monitoring. Y.L. conducted finite element simulation and contributed to design of auxetic dumbbell hole patterns. J.L. and Y.-C.J. evaluated mechanical properties and reliability of e-skins. B.S.M. and T.-S.K. evaluated adhesion of e-skins. J.H. and E.K. led clinical study including skin compatibility test of e-skin and evaluation of e-skin breathability on the forearm. All authors discussed and contributed to the discussion and analysis of the results regarding the manuscript at all stages. **Competing interests:** The authors declare that they have no competing interests. **Data and materials availability:** All data needed to evaluate the conclusions in the paper are present in the paper and/or the Supplementary Materials.

Submitted 4 February 2021
Accepted 17 May 2021
Published 30 June 2021
10.1126/sciadv.abg8459

Citation: H. Yeon, H. Lee, Y. Kim, D. Lee, Y. Lee, J.-S. Lee, J. Shin, C. Choi, J.-H. Kang, J. M. Suh, H. Kim, H. S. Kum, J. Lee, D. Kim, K. Ko, B. S. Ma, P. Lin, S. Han, S. Kim, S.-H. Bae, T.-S. Kim, M.-C. Park, Y.-C. Joo, E. Kim, J. Han, J. Kim, Long-term reliable physical health monitoring by sweat pore–inspired perforated electronic skins. *Sci. Adv.* **7**, eabg8459 (2021).